Hindawi
International Journal of Antennas and Propagation
Volume 2019, Article ID 4890710, 11 pages
https://doi.org/10.1155/2019/4890710

Research Article

Modified Minkowski Fractal Unit Cell for Reflectarrays with Low Sensitivity to Mutual Coupling Effects

Sandra Costanzo, Francesca Venneri, and Giuseppe Di Massa

Università della Calabria, Rende, Italy

Correspondence should be addressed to Sandra Costanzo; costanzo@dimes.unical.it

Received 30 July 2018; Revised 25 November 2018; Accepted 23 December 2018; Published 18 February 2019

Academic Editor: Jaume Anguera

A single-layer miniaturized reflectarray element with low sensitivity to mutual coupling effects of surrounding elements is presented in this paper. The configuration is proposed to preserve the effectiveness of the infinite array approach in those applications requiring reflectarrays with very small interelement spacing. The inherent ability of the proposed geometry to be adopted in highly miniaturized cells is demonstrated through an extensive analysis of mutual coupling effects on reflectarray phase design curves. In order to prove the independence of the proposed cell to mutual coupling effect, the phase curve variations due to the presence of different surrounding elements with respect to the case of identical cells are evaluated using the well-known extended local periodicity method. Small and negligible mutual coupling errors are retrieved for the proposed miniaturized unit cell, thus demonstrating lower sensitivity to mutual coupling adverse effects.

1. Introduction

Reflectarray antennas proved their effectiveness for several applications, going from space exploration to wireless communication systems [1–7]. As well known, the basic structure consists of an array of microstrip radiators illuminated by a feed antenna. Each reflectarray cell is designed to reradiate the impinging field with a given phase delay. In order to comply with this task, the geometrical/electrical features of the single-unit cell must be properly tuned to achieve a full phase control of the reradiated field.

Strictly speaking, the above operational principle implies a rather complicated design procedure that involves the reiteration of the unit cell response analysis when it is surrounded by differently shaped/sized elements, according to its location in the array grid. This kind of analysis approach, such as that based on the finite-difference time domain (FDTD) proposed in [8] or the extended local periodicity (ELP) discussed in [9], becomes impractical for large reflectarray design.

Although the above methods allow to give a rigorous estimation of mutual coupling effects due to different neighboring elements, the most efficient method usually adopted for the reflectarray analysis is the infinite array periodic approach based on Floquet's theorem [1]. Actually, this method reduces the analysis to one periodic cell, by automatically taking into account the mutual coupling between identical elements, thus providing a quite good prediction of the unit cell response in the array environment. Nonetheless, some situations could make the infinite array approach inadequate for the unit cell analysis and design. For example, the use of very small interelement spacing ($<\lambda/2$) [10, 11], which is essential for wide-angle beam scanning design, gives rise to higher and very dissimilar mutual coupling levels between different unit cell occurrences, due to the very small separations between patches.

The aim of this paper is to overcome the above difficulties, by proposing the adoption of a miniaturized linearly polarized unit cell with uniform mutual coupling levels, therefore able to meet the periodic boundary conditions imposed by Floquet's theorem [1].

To this end, a modified layout of the fractal unit cell, originally introduced by the authors in [12, 13], is investigated and discussed in this paper to increase the unit cell

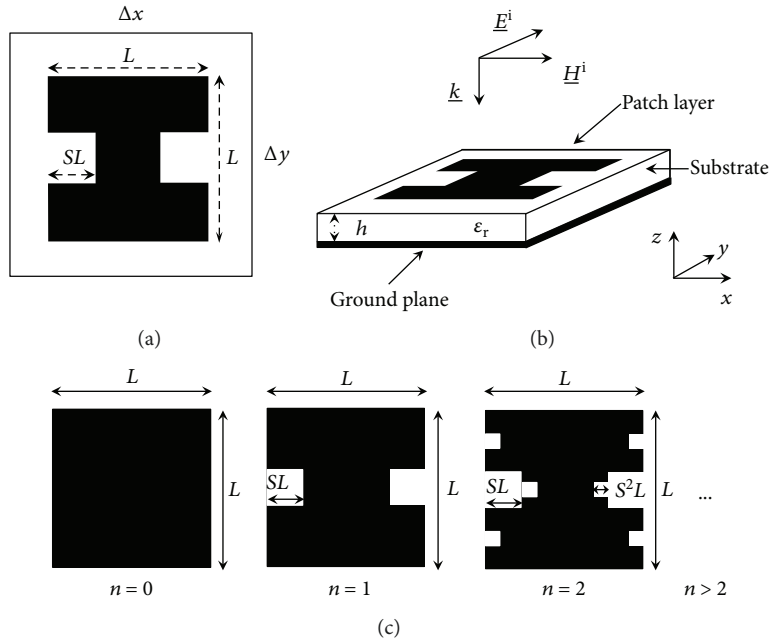

Figure 1: Layout of the proposed unit cell: (a) top view; (b) 3D view and reference system; (c) fractal construction.

insensitivity to mutual coupling, thus preserving the effectiveness of the infinite array approach, even in the case of highly miniaturized reflectarray cells.

Other reflectarray configurations allow to achieve nearly constant mutual coupling, such as the well-established configurations based on the use of fixed-size rectangular patches attached (or aperture coupled) to delay lines [1, 10], the fixed-size Minkowski patch with a variable slot in the ground plane [14], and the dual-band Phoenix cell proposed in [15]. Apart from the first mentioned configuration, not suitable for miniaturization purpose (the use of very small cells ($<\lambda/2$) is not always able to host a printed variable phasing line on the same patch layer), the above configurations give interesting solutions for designing miniaturized reflectarray cells.

Despite the above reflectarray cells, the configurations proposed in this work allow very high miniaturization degrees, by offering, at the same time, single-layer and thinner profiles, good phase swings, and lower reflection losses. All these appealing features, in the case of the abovementioned configurations, can be achieved only by adopting an additional $\lambda/4$-spaced metal plate, for back-radiation mitigation, or by increasing the substrate thickness, including an air layer. Furthermore, as demonstrated in [16–19] for other X-band subwavelength reflectarrays, printed on $\lambda/10$-thick substrates, the joint use of subwavelength unit cells and thicker substrate layers can lead to the design of broadband reflectarrays [1, 10].

The unit cell independence to mutual coupling is evaluated through the ELP approach, by computing the phase curve variations due to the presence of different surrounding elements with respect to the case of identical cells. The above variations give a measure of the intrinsic error due to the infinite array approximations. Smaller and negligible phase errors are observed in the case of the proposed element, when a miniaturized unit cell is considered, so that the infinite array approach can be effectively adopted to derive the phase design curves, without affecting the accuracy of the reflectarray synthesis stage. Furthermore, in order to give a physical interpretation of mutual coupling between reflectarray cells, a simple transmission line model (TL model) is adopted for the unit cell analysis [20]. The model, consisting of a RLC series circuit, is used to derive the mutual coupling behavior from the unit cell capacitance C, which is essentially related to the contribution of parasitic capacitors between the edges of adjacent patches [20], and therefore is strictly related to unit cell mutual coupling levels. The analysis shows that the C values associated to the proposed fractal cells, as compared with those relative to a standard variable square patch, reveal a much more stable behavior vs the corresponding phase tuning parameter, thus confirming the results achieved in terms of phase curve errors.

The paper is organized as follows. Section 2 describes the general design details of the proposed reflectarray elements. In Section 3, the performances of a set of miniaturized fractal unit cells are illustrated and compared with those related to standard variable square unit cells [21]. Section 4 describes the results of a mutual coupling analysis on the proposed unit cells. Section 5 shows some subwavelength reflectarray designs, demonstrating the lower sensitivity of the proposed cell to mutual coupling adverse effects. Conclusions are finally outlined in Section 6.

2. Reflectarray Unit Cell Geometry

The proposed reflectarray unit cell is depicted in Figure 1(a). Its layout is essentially derived from the 1st iteration fixed-length Minkowski patch originally proposed by the authors in [12]. The patch geometry reported in Figure 1(a) is characterized by a beginning square element of dimensions $L \times L$. Unlike the Minkowski fractal patch, a smaller square of

Table 1: Fractal unit cell performances.

Cell type	Cell size $\Delta x = \Delta y$	Patch length L (mm)	Variable scaling factor S	Phase range (deg)	$\Delta x - L$ (mm)
Proposed element (Figure 1(a))	0.6λ	7.75	$0 \div 0.45$	355	10.25 (~0.342λ)
	0.5λ	7.75	$0 \div 0.45$	350	7.25 (~0.242λ)
	0.4λ	7.72	$0 \div 0.45$	348	4.28 (~0.143λ)
	0.3λ	7.46	$0 \div 0.45$	330	1.54 (~0.051λ)
Minkowski element [12]	0.6λ	7.86	$0 \div 0.325$	350	10.14 (~0.338λ)
	0.5λ	7.86	$0 \div 0.325$	345	7.14 (~0.238λ)
	0.4λ	7.82	$0 \div 0.325$	340	4.18 (~0.14λ)
	0.3λ	7.6	$0 \div 0.325$	320	1.4 (~0.047λ)

side SL is removed only from the center of the two lateral sides (namely, the resonant sides, if assuming a TE^x impinging wave (see Figure 1(b)), thus obtaining a linearly polarized cell along the y-axis. The reflection-phase tuning is realized by varying the fractal scaling factor S from 0 up to 0.45 and leaving unchanged both the patch length and the separation distance between adjacent patches (i.e., $\Delta x - L$ in Figure 1).

As in [12, 22, 23], the fractal construction can be infinitely reiterated to obtain an increasingly complex self-similar shape, according to the construction rule described above and depicted in Figure 1(c), where the results of the first two iterations are shown.

The main benefit derived from the adoption of the above fractal geometries is related to the fact that more electrical length can be fitted into a smaller physical area [22]. Of course, the increased electrical length of fractal patches (i.e., $L_n = (1 + 2nS)L$ for the proposed patch (Figure 1(a)), $L_n = (1 + 2S)^n L$, for the Minkowski patch in [12, 22]) leads to lower resonant frequencies, so that fractal antennas should be miniaturized in order to obtain the resonance at the desired operating frequency. In addition to the above features, the novel patch layout allows to slightly enlarge the phase tuning range due to the increased variation range of the scaling factor S, which is not limited by the upper-bound $L/3$ as in the case of the Minkowski patch [12]. Furthermore, as it will be demonstrated in the following sections, the fixed length of the radiating sides (i.e., upper and lower sides of the patch in Figure 1(a)) guarantees a higher independence to mutual coupling effects. As a matter of fact, literature [24] demonstrates how the stronger contribution to the mutual coupling between microstrip patches is that occurring along the E plane (yz plane in Figure 1(b)). So, leaving unchanged both the shape and the separation distance between the patches in the E plane (Figure 1(a)), a quite uniform mutual coupling level between the reflectarray unit cells can be assured. This last feature provides several benefits that will be discussed in the following sections.

3. Design and Comparative Performance Evaluation of Reflectarray Unit Cell

To investigate the effects due to the unit cell size reduction of the proposed fractal configurations, a set of 10 GHz reflectarray unit cells is designed by varying the cell size Δx from 0.6λ down to 0.3λ. The antennas are printed on a Diclad870 substrate ($\varepsilon_r = 2.33$) having a thickness $h = 0.762$ mm (Figure 1(b)). A commercial full-wave code [25], based on the method of moments, is adopted for the analysis of the cells, assuming a normal incident plane wave as source and adopting the infinite array analysis tool.

Each cell is designed by following the design rules outlined in [12], namely, the patch length L is properly fixed to achieve the resonance at 10 GHz for a given value of S (i.e., $S = 0.2$), while the phase tuning is realized by varying S from 0 up to 0.45, for the proposed cell in Figure 1(a), and from 0 up to 0.325, for the Minkowski cell [12]. The geometrical features as well as the performances of each designed cell are reported in Table 1. Comparisons with data relative to standard variable square patch cells printed on the same substrate are also reported in Table 2. In this last case, the phase tuning is achieved through a ±30% patch size sweep with respect to the patch resonant length L_{res}.

At a glance, smaller patch dimensions are observed in the case of fractal elements (Table 1), corresponding to a 15%÷ 19% size reduction with respect to the resonant length of the 0.6λ cell-embedded square patch (i.e., $L_{res} = 9.215$ mm in Table 2). Furthermore, fractal cells offer quite good phase ranges (≥330° for the proposed patch in Figure 1(a); ≥320° for the Minkowski patch [12]). These are greater than those relative to the equivalent variable square-based cells (see Tables 1 and 2).

On the other hand, Table 2 reveals that, in the case of very small cells (i.e., $\Delta x < 0.5\lambda$), the standard variable square patch configuration shows the following limitations: (a) the cell dimension strongly restricts the achievable phase range due to the size constraints imposed on the patch side length variations (e.g., only 283° for the 0.3λ cell) and (b) as it is well known from literature [24], the heavy variations in the gap distance between adjacent patches (i.e., $\Delta x - L$ in Figure 1), varying, for example, from 0.009λ up to 0.19λ in the case of the 0.4λ cell (Table 2), cause very dissimilar mutual coupling levels that make unreliable periodic boundary conditions for reflectarray cell simulations.

Thanks to the proposed phase tuning approach, leaving unchanged the element side length (i.e., the gap $\Delta x - L$ in Table 1), the proposed fractal cells overcome the above limitations, confirming themselves as good candidates for miniaturization purpose. Furthermore, as it can be observed

Table 2: Variable square unit cell performances.

Cell size $\Delta x = \Delta y$	Resonant patch length L_{res} (mm)	Patch length variation (mm) $L = L_{res} \pm 30\% L_{res}$	Phase range (deg)	Min$(\Delta x - L)$ (mm)	Max$(\Delta x - L)$ (mm)
0.6λ	9.215	6.45 ÷ 12	336	6 (~0.2λ)	11.55 (~0.39λ)
0.5λ	9.15	6.4 ÷ 11.9	328	3.1 (~0.1λ)	8.6 (~0.29λ)
0.4λ	9.02	6.3 ÷ 11.73	322	0.27 (~0.009λ)	5.7 (~0.19λ)
0.3λ	8.3	5.8 ÷ 8.8 (i.e., $6\% L_{res}$)	283	0.2 (~0.007λ)	3.2 (~0.11λ)

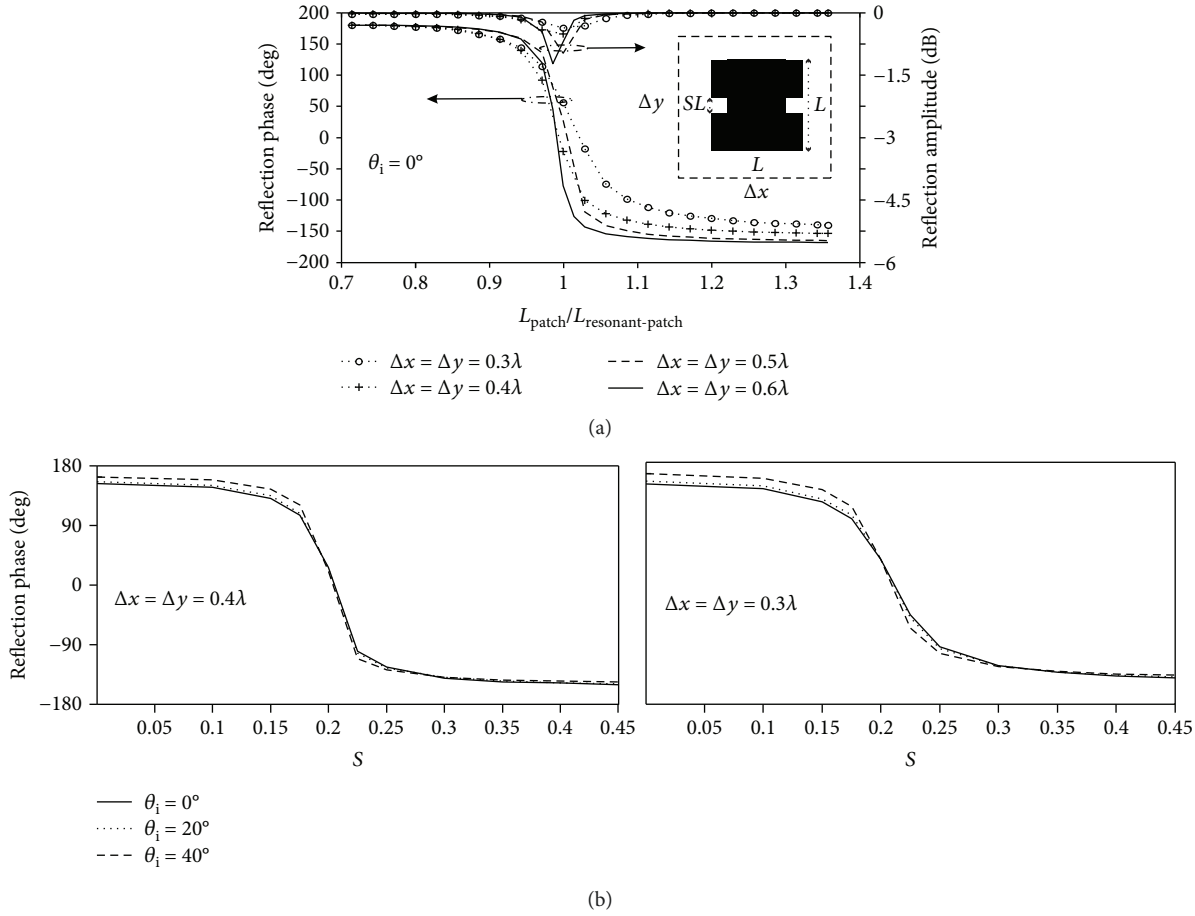

Figure 2: Reflection coefficient for different cell sizes of the proposed configuration (Figure 1): (a) vs $L_{patch}/L_{resonant-patch}$ ($L_{resonant-patch} = (1 + 2 \times 0.2)L$) and $\theta_i = 0°$; (b) vs S for different incidence angles θ_i.

in the reflection coefficient curves (Figure 2(a)) computed for different cell sizes vs the effective patch length $L_{patch} = (1 + 2S)L$, the use of smaller cells improves reflectarray bandwidth, fabrication tolerance, and loss performances (e.g., reflection losses lower than 0.3 dB for $\Delta x = 0.3\lambda$). Figure 2(b) also shows acceptable phase variations under 20° and 40° oblique incidence, with respect to the normal case. As a further advantage, the proposed configuration in Figure 1(a) shows very low cross-polar components, as illustrated in Figure 3, where both the copolar as well as the cross-polar patterns are computed for different scaling factor values (i.e., $S = 0, 0.2$), in the case of the miniaturized unit cells (i.e., $\Delta x < 0.5\lambda$) of Table 1.

4. Mutual Coupling Analysis of Reflectarray Cells

Due to their quasiperiodicity feature, reflectarrays are usually analyzed and designed under the infinite periodic array assumption [1]. However, if the different unit cell instances (necessary to achieve a quite full 360° reflection phase control) exhibit very dissimilar behaviors in terms of mutual coupling, data derived from the infinite array analysis cannot be used to properly characterize a single-unit cell, as not leading to a correct reflectarray design [8, 9, 26]. This issue becomes more relevant in those applications requiring unit cell miniaturization. In order to demonstrate the poor

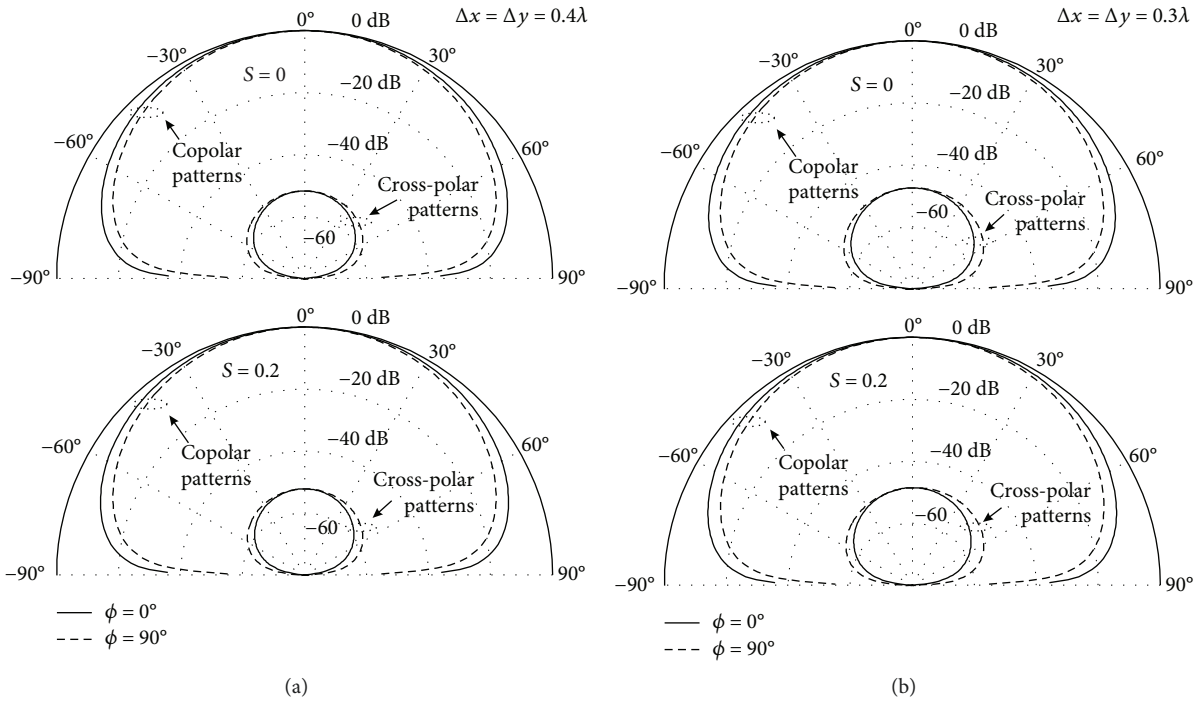

Figure 3: Copolar and cross-polar patterns of the proposed configuration (Figure 1(a)) for different S values: (a) $\Delta x = \Delta 0.4\lambda$; (b) $\Delta x = 0.3\lambda$.

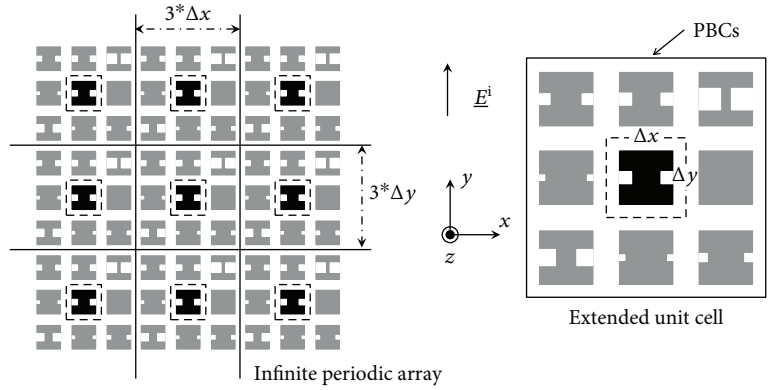

Figure 4: Modeling of an infinite periodic array and the extended unit cell with the imposed periodic boundary conditions (PBCs) [27].

sensitivity of the proposed fractal configuration (Figure 1) to mutual coupling adverse effects, an extensive analysis of mutual coupling behavior is reported in the following. In particular, the first subsection shows the phase errors in the mutual coupling estimation due to the infinite array approach, as compared to the real situations where the unit cell is surrounded by different radiators. In the second subsection, the mutual coupling behavior is explained through the implementation of an equivalent transmission line model for the reflectarray unit cells.

4.1. Mutual Coupling Phase Error Evaluation. In order to evaluate the mutual coupling effects on the phase response of reflectarray cells, the phase design curves are computed by adopting the ELP approach proposed in [9]. The method is essentially equivalent to the infinite array approach, with the periodicity conditions (PBCs [1, 27]) applied to an extended unit cell, which includes the actual surrounding elements (Figure 4). The extended unit cell includes the nearest eight surrounding elements in the reflectarray grid. The method is adopted to compute the phase curve variations $\Delta\phi$ due to the presence of different surrounding elements with respect to the case of identical elements.

A commercial full-wave code [25] is adopted to simulate the periodic extended cell (Figure 4) and to evaluate the current density $\underline{J}_s$ induced on the central patch (enclosed in Figure 4 within the dashed lines) when assuming a normally incident plane wave. The so-computed current takes into account the right mutual coupling due to the actual surrounding patches. Afterwards, the current density $\underline{J}_s$ is extrapolated from the code, in order to calculate the electric far field $\underline{E}^s_{\text{patch}}$ radiated by the central patch, through the

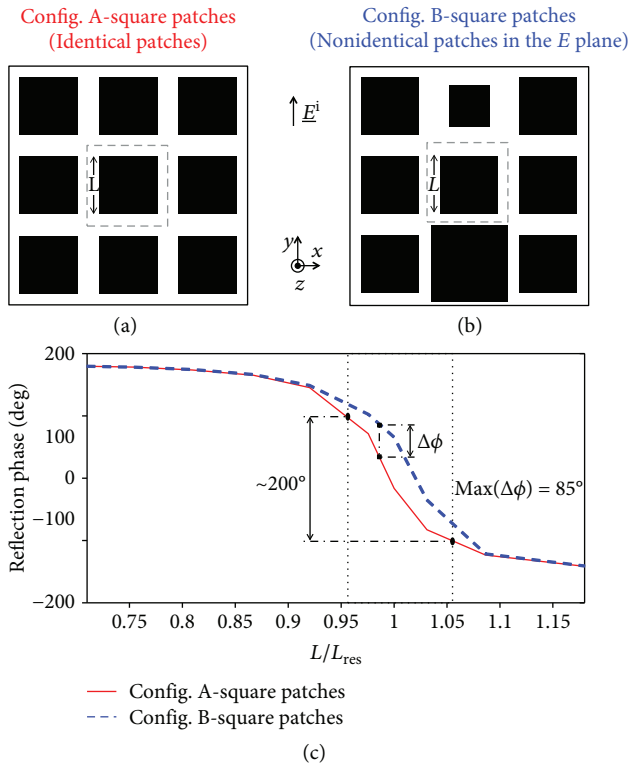

FIGURE 5: Phase design curves vs the normalized patch length (i.e., L/L_{res}—see Table 2) simulated for different surrounding patch configurations: (a) config. A—identical square-based cells; (b) config. B—nonidentical square-based cells in the E plane; (c) phase curve comparisons.

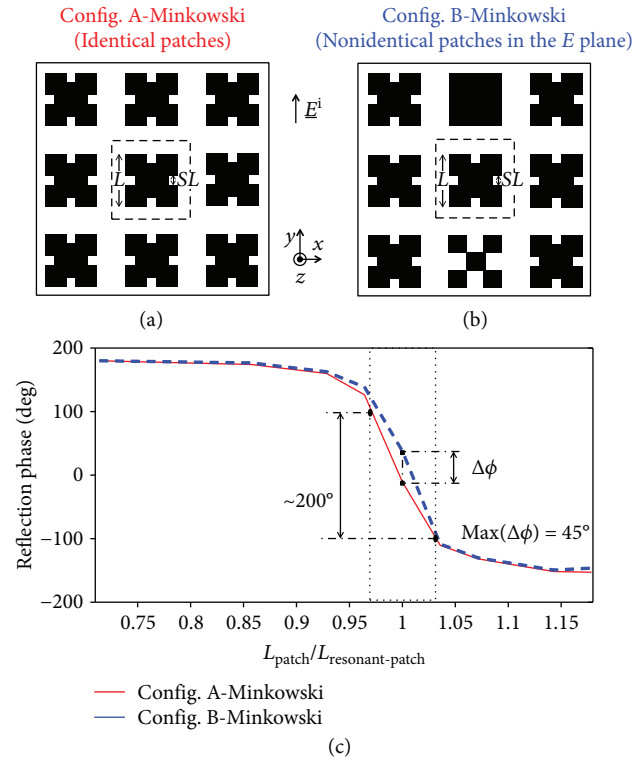

FIGURE 6: Phase design curves vs the normalized patch length (i.e., $L_{patch}/L_{resonant-patch} = ((1 + 2S)L)/((1 + 2*0.2)L)$—see Table 1) simulated for different surrounding patch configurations: (a) config. A—identical Minkowski cells; (b) config. B—nonidentical Minkowski cells in the E plane; (c) phase curve comparisons.

implementation of the auxiliary vector potential $\underline{A}$ formula [24], i.e., by solving the integral $\underline{A}(x, y, z) = (\mu/4\pi) \iint_s \underline{J}_s(x', y')(e^{-j\beta R}/R)dS'$ over the patch surface S', where the primed coordinates represent the source, while the unprimed coordinates indicate the observation point, and R is the distance from any source point to the observation point. After that, the radiated field is computed trough the formula $\underline{E} = -j\omega A$ [24], valid in the far field region. The so-computed electric far field $\underline{E}^s_{patch}$ is finally added to the contribution $\underline{E}^s_{ground}$ scattered by the ground plane of size $\Delta x \times \Delta y$ (Figure 4), which is embedded into the cell and evaluated by the physical optics theory [28]. The phase design curves are computed as the phase of the total field reflected from the unit cell $\underline{E}^s_{tot} = \underline{E}^s_{patch} + \underline{E}^s_{ground}$, by varying the central patch length (i.e., the scaling factor S), for a given configuration of the surrounding elements. The above method is applied to evaluate the phase design curves at $f_0 = 10$ GHz, for the miniaturized cells of Tables 1 and 2 having $\Delta x = \Delta y = 0.4\lambda$. Two different surrounding element configurations are considered for each cell type (i.e., the variable square patch in Figure 5, the Minkowski element in Figure 6, and the configuration proposed in this work (Figure 7)).

In particular, to effectively evaluate the mutual coupling contribution on the phase response of each considered unit cell type, a first configuration (A) with identical surrounding elements (Figures 5(a), 6(a), and 7(a)), equivalent to the infinite array approximation, is compared with a configuration (B) having two nonidentical elements in the E plane (Figures 5(b), 6(b), and 7(b)). To assess the worst case, two fixed elements are considered, having, respectively, the maximum and the minimum patch lengths (Figure 5(b)) and the maximum/minimum scaling factor S (Figures 6(b) and 7(b)). For the sake of simplicity, only the results relative to E plane nonidentical elements (Figures 5(b), 6(b), and 7(b)) are illustrated, as they give higher mutual coupling levels [24] and consequently higher phase errors with respect to the H plane case. Finally, in the case of the configuration proposed in this paper, a maximum phase excursion $\Delta\phi$ just equal to 20° is achieved (Figure 7(c)) between the phase curves computed for the two considered extended cell configurations (Config. A—Figure 7(a) and Config. B—Figure 7(b)). It occurs only in correspondence of a very small neighborhood of the ratio $L_{patch}/L_{resonant-patch} \cong 0.96$ (i.e., $S \cong 0.175$). Furthermore, the current distributions computed on the central elements for $S = 0.175$ (i.e., the worst case) are almost identical (Figure 8(b)). This last result shows that the modified patch of Figure 1 exhibits an invariant mutual coupling behavior, thus better satisfying the periodic boundary conditions of the usually adopted infinite array analysis approach, also in the case of miniaturized cells ($\Delta x < \lambda/2$). Table 3 shows the maximum phase errors given by the ELP approach applied to different unit cell sizes. Smaller and negligible phase errors

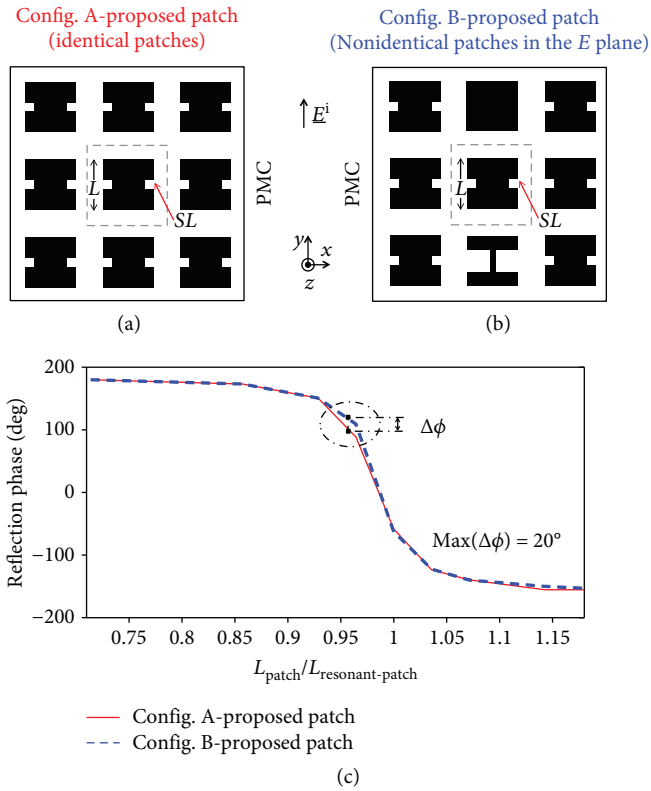

FIGURE 7: Phase design curves vs the normalized patch length (i.e., $L_{patch}/L_{resonant-patch} = ((1+2S)L)/((1+2^{*}0.2)L)$—see Table 1) simulated for different surrounding patch configurations: (a) config. A—identical proposed cells; (b) config. B—nonidentical proposed cells in the E plane (c); phase curve comparisons.

are observed in the case of the proposed element, when a miniaturized unit cell is considered, so that the infinite array approach can be effectively adopted to derive the phase design curves.

4.2. Circuit-Based Model for the Interpretation of Mutual Coupling in Reflectarray Antennas. A circuit model approach is adopted to give a qualitative interpretation of mutual coupling between reflectarray unit cells, by also justifying the quantitative results in terms of phase errors achieved in the previous paragraph. The TL model approximation is already adopted in [20] for the analysis of some standard reflectarray radiators (i.e., dipole, ring, and square patch) to clarify the mechanism causing reflection losses in reflectarrays. The layout of the analyzed structure and its equivalent circuit are reported in Figure 9.

The equivalent circuit parameters are retrieved from a MoM simulation, by matching the impedance Z_{cell} (Figure 9(b)) with that derived from the simulated reflection coefficient [20, 29]. The main purpose of the equivalent TL model is to retrieve, from the cell capacitance behavior, the effects due to the geometrical phase tuning parameters (i.e., the scaling factor S for the proposed configurations) on the mutual coupling among elements. As a matter of fact, the capacitance C is strictly related to the interaction between the edges of adjacent patches where the excited electric field is stronger [20], so it gives information about the mutual coupling behavior. The extrapolation procedure is applied to all designed cells described in Section 3 (see Tables 1 and 2), in order to investigate the impact of fractal cell miniaturization on the capacitance values.

Figure 10 depicts the capacitance of each cell considered in previous tables. The data are organized as follows. Each curve refers to a fixed cell size ranging from 0.6λ down to 0.3λ. The solid and the dotted curves represent, respectively, the capacitance of the Minkowski and the proposed cells computed by varying the scaling factor S (Table 1), while the dashed curves show the capacitance behavior of variable square patch-based cells (Table 2). Both solid/dotted and dashed curves are plotted vs the normalized length $L_{patch}/L_{resonant-patch}$, which is equal to the ratio $(1+2S)/(1+2\times 0.2)$ in the case of fractal patches, while it is equal to the ratio L/L_{res} in the case of variable square patches. It can be observed that both fractal cell capacitances decrease when S increases, as the distance between two adjacent element edges becomes greater in correspondence to the inset SL (see Figure 1).

The opposite behavior can be appreciated in the capacitance of square patches, as greater patch lengths give smaller gap distances between adjacent elements, namely, an increasing capacitive coupling. Anyway, the main result demonstrated in Figure 10 is that, for a fixed cell size, both fractal patch configurations are characterized by slower capacitance variations. As a matter of fact, the capacitance variation exhibited by the variable square-based cells is about 20 times larger than that provided by the corresponding fractal cells (Figure 10). Furthermore, in the case of the cell proposed in this work (Figure 1), a quite constant capacitance value can be observed vs the scaling factor variations.

This higher stability, in terms of cell capacitance, is guaranteed by the fixed radiating sides (i.e., the upper and lower sides of the patch in Figure 1(a)) that assure a quite stable mutual coupling level between reflectarray cells. In conclusion, the analyzed fractal configurations are characterized by uniform mutual coupling levels, also in the case of miniaturized cells, so that the proposed fractal cells, in particular the novel configuration of Figure 1(a), satisfy very well the infinite array approximation.

5. Reflectarray Designs

In order to test the large-angle pointing capability of the proposed miniaturized cells and to better illustrate the advantages derived by their intrinsic uniform mutual coupling, three reflectarray antennas are designed based on the use of the proposed cell (Figure 11(a)), the Minkowski patch (Figure 11(b)), and the variable size patch (Figure 11(c)). All prototypes consist of 15×15 0.3λ spaced elements, illuminated by an offset horn with a 15° tilt angle in the E plane (yz plane in Figure 11(d)). The array is realized with a printed circuit board (PCB) milling machine [30]. The feeding horn, having an aperture size equal to 4.8 mm × 5 mm, is placed at a distance equal to 50 cm from the array, thus satisfying the far field condition. The antennas are synthesized [26] to

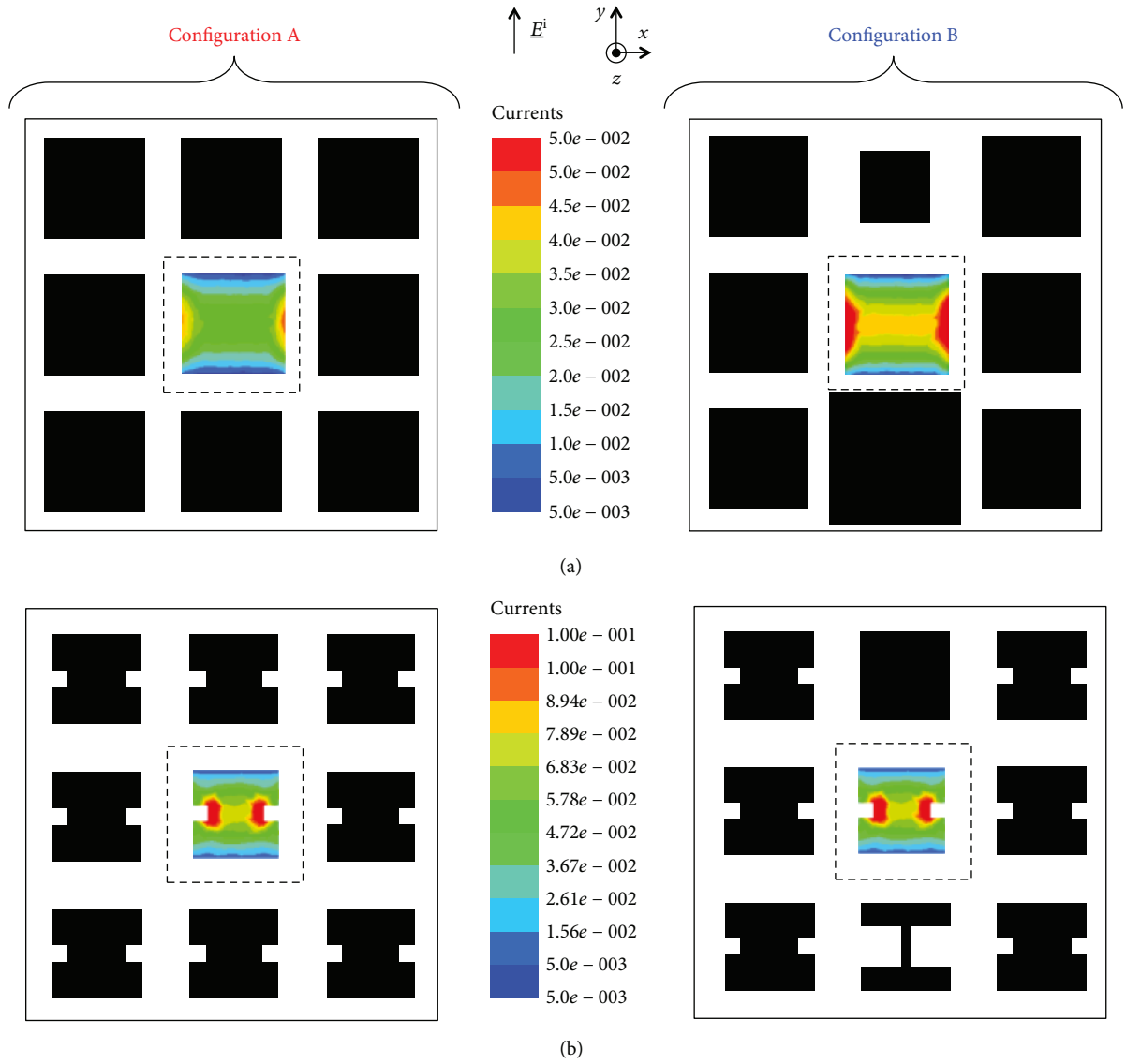

Figure 8: Central element current distributions for different surrounding element configurations: (a) square-based cells; (b) proposed cells.

Table 3: Phase range and error evaluation through the ELP approach.

Cell size	Square-based cell		Minkowksi cell		Proposed cell	
	Phase range	Max($\Delta\phi$)	Phase range	Max($\Delta\phi$)	Phase range	Max($\Delta\phi$)
0.5λ	336°	25°	342°	21°	345°	12°
0.4λ	330°	>45°	332°	≅45°	340°	20°
0.3λ	288°	>45°	310°	≅45°	326°	34°

focalize the main beam along the direction $\theta_{MB} = 48°$, in the H plane (i.e., the xz plane in Figure 11). As it can be observed in the front view of the synthesized examples (Figures 11(a)–11(c)), each (n, m) element is characterized by different sizes, namely, a specific scaling factor S_{nm} and/or patch length L_{nm}, which are properly chosen to compensate for the phase delay in the field coming from the feed and to get also the prescribed pattern.

A synthesis algorithm based on the iterative projection method [26] is applied to compute the phase distribution on the array elements satisfying the imposed design goals on the radiation pattern, in terms of upper- and lower-bound masks [26].

The algorithm automatically returns the required excitation phase ϕ_{nm} on each reflectarray element. This last data are finally adopted to select the elements sizes S_{nm} and/or L_{nm}, by using the design curves, which are simulated under the infinite array approach assumption (Figures 5(a)–7(a)). To this end, a research routine is implemented that fits the desired ϕ_{nm} values onto the simulated phase curves (Figures 5(a)–7(a)), finally returning the corresponding scaling factors S_{nm} or the patch lengths L_{nm}. A more detailed description of the implemented research routine is reported in [13].

Figure 11(e) illustrates the comparison between the radiated H plane patterns. The measurements are performed with a far field facility (Figure 11(d)) connected to a VNA (Anritzu 37217C). An X-band horn is adopted as probe

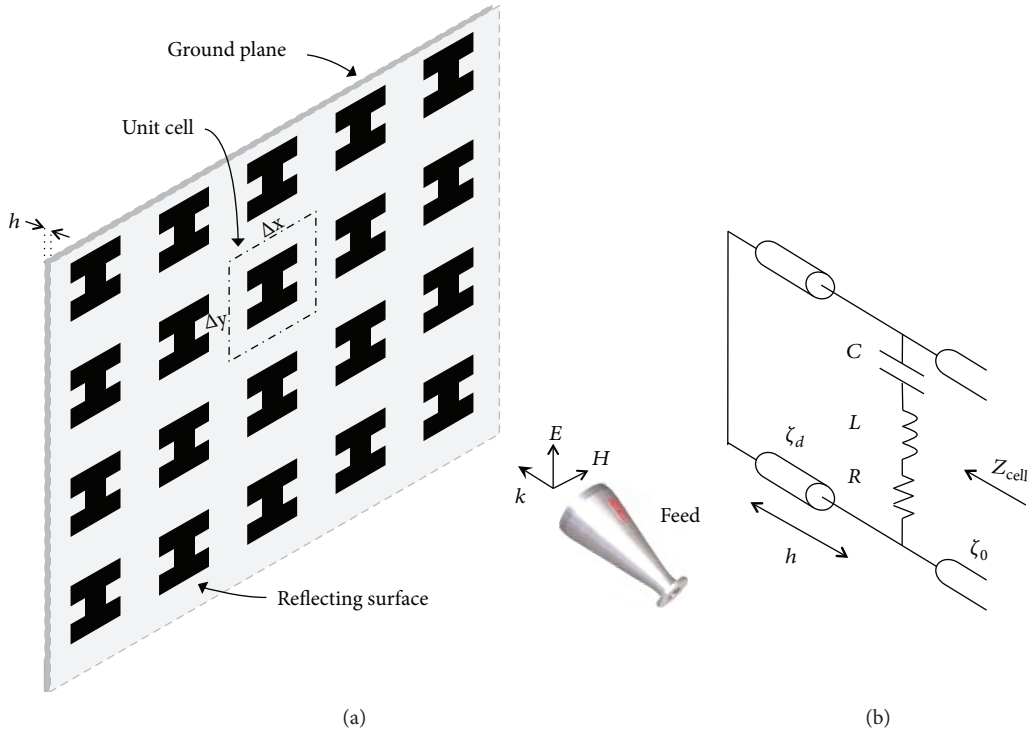

Figure 9: Analyzed structure: (a) 3D layout of a periodic fractal reflectarray; (b) unit cell equivalent circuit.

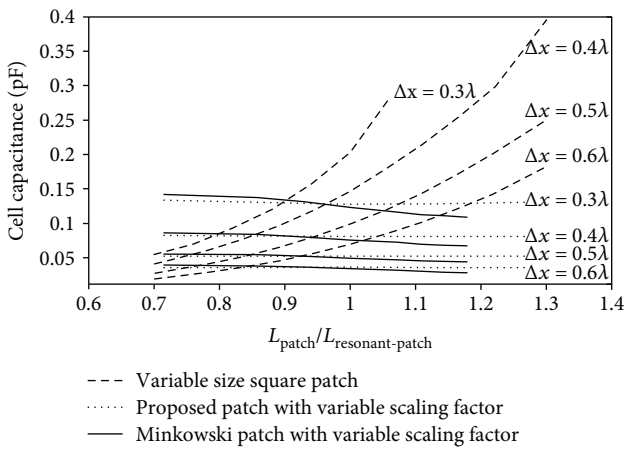

Figure 10: Comparison between cell capacitances computed for fractal and square patches by varying the phase tuning parameter for different cell sizes.

and is placed in front of the reflectarray aperture, at a distance satisfying the far field condition [24]. In order to detect the H plane radiation patterns, the antennas under test are properly rotated around their axis (i.e., y-axis in Figure 11(d)), from -90° up to 90°. It can be observed how the proposed configuration in Figure 11(a) allows to scan the main beam along the desired direction, by maintaining low side lobes (i.e., SLL<−13 dB), thus confirming the effectiveness of the infinite array analysis for the phase design curve computation. As a matter of fact, the smaller phase error characterizing the proposed cell (see Section 4), due to infinite array approximations, does not affect the antenna radiation performances. On the contrary, in the case of the Minkowski-based reflectarray (Figure 11(b)), the phase errors characterizing the adopted phase design curve ($\Delta\phi \leq 45^\circ$—see Section 4) give a radiation pattern exceeding the SLL constraints of 2.5 dB, in correspondence of the first side lobe, and equal to about 1.2 dB along $\theta = -17^\circ$. Finally, in the case of the square-based reflectarray (Figure 11(c)), the higher phase errors ($20^\circ \leq \Delta\phi \leq 85^\circ$—see Section 4) characterizing the adopted design curve give very high side lobes (e.g., ≅−8 dB, along $\theta = 0^\circ$ and ≅ −6.4 dB, along $\theta = -18^\circ$) which exceed the SLL constraint up to a value of 6.6 dB over (see the dotted pattern in Figure 11(e)). Furthermore, a 0.75 dB gain reduction is observed in the gain of the square-based reflectarray that, considering the constant spillover and tapering losses [1] characterizing all designed antennas, causes an aperture efficiency reduction of about 15% with respect to the proposed configuration.

6. Conclusion

A novel fractal reflectarray radiator has been proposed in this work to design miniaturized reflectarray cells having good performances in terms of phase variation and mutual coupling behavior, useful for wide-angle beam-steering applications. The benefits offered by the proposed cell with respect to the most widely adopted variable square reflectarray configuration have been discussed. Furthermore, an extensive analysis of mutual coupling effects on the reflectarray phase design curve has been performed. The proposed reflectarray cell exhibits uniform mutual coupling levels vs its geometry variations, thus satisfying the periodic boundary conditions imposed by Floquet's theorem, without occurring into phase

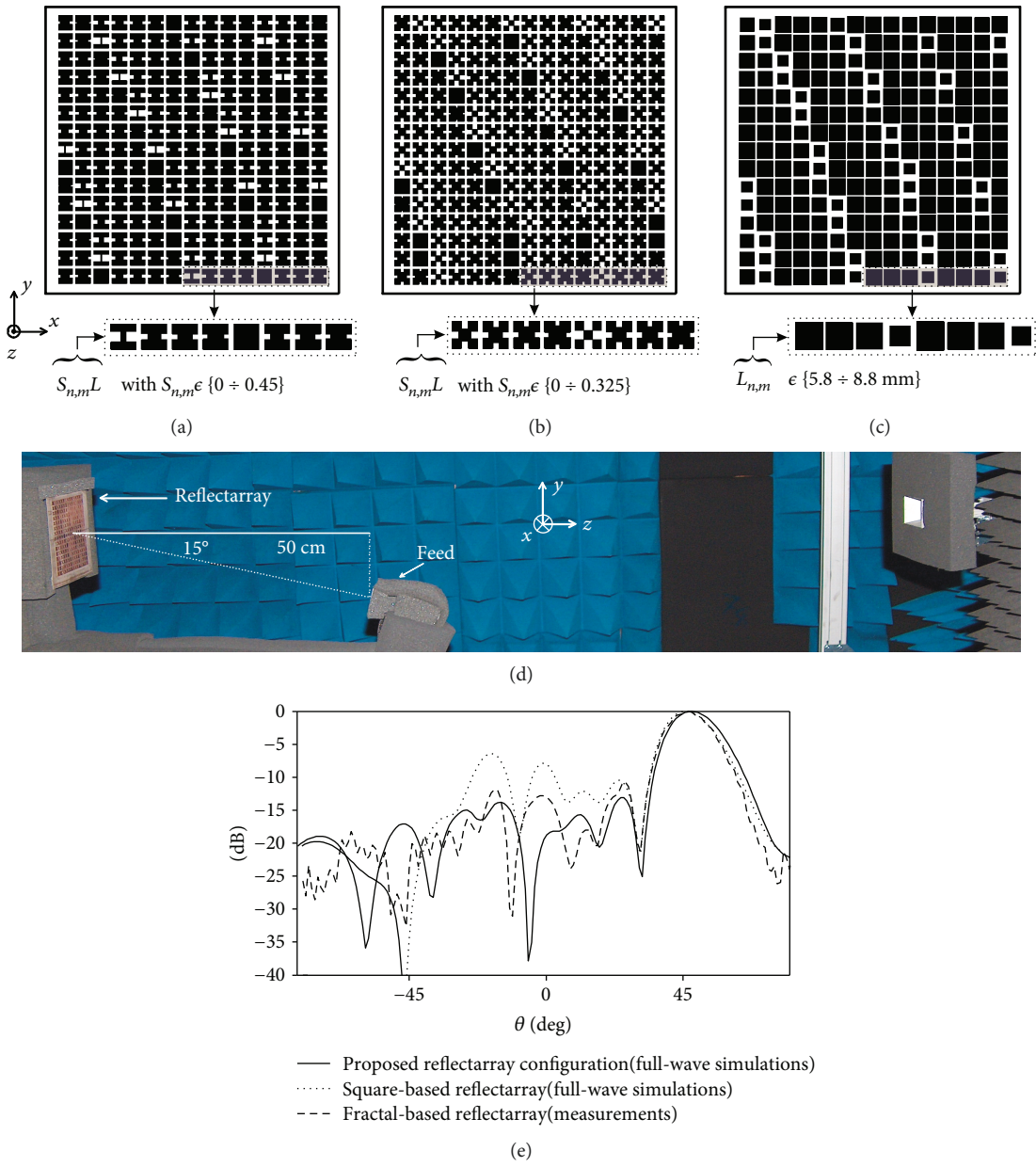

Figure 11: Designed reflectarray prototypes: (a) proposed configuration; (b) Minkowski cells; (c) square-based cells; (d) far field measurement setup; (e) H plane radiation patterns.

curve estimation errors, and confirming itself as a promising solution for subwavelength reflectarray applications. Finally, the subwavelength reflectarray designs, reported in Section 5, have confirmed the results achieved during the analysis stage. As a matter of fact, the smaller phase curve errors characterizing the proposed cell, due to infinite array approximation, do not affect the radiation performances of the synthesized antenna, so we can conclude that the proposed miniaturized configuration meets very well the infinite array assumption.

Data Availability

The data used to support the findings of this study are included within the article.

Conflicts of Interest

The authors declare that they have no conflicts of interest.

References

[1] J. Huang and J. Encinar, *Reflectarray Antennas*, Wiley-IEEE Press, 2008.

[2] S. V. Hum and J. Perruisseau-Carrier, "Reconfigurable reflectarrays and array lenses for dynamic antenna beam control: a review," *IEEE Transactions on Antennas and Propagation*, vol. 62, no. 1, pp. 183–198, 2014.

[3] F. Yang, P. Nayeri, and A. Z. Elsherbeni, "Recent advances in beam-scanning reflectarray antennas," in *2014 XXXIth URSI*

General Assembly and Scientific Symposium (URSI GASS), pp. 1–4, Beijing, China, 2014.

[4] S. Costanzo, "Reflectarray antennas: analysis and synthesis techniques," *International Journal of Antennas and Propagation*, vol. 2012, Article ID 945682, 3 pages, 2012.

[5] F. Venneri, S. Costanzo, and G. Di Massa, "Reconfigurable aperture-coupled reflectarray element tuned by single varactor diode," *Electronics Letters*, vol. 48, no. 2, pp. 68-69, 2012.

[6] F. Venneri, S. Costanzo, and G. Di Massa, "Design and validation of a reconfigurable single varactor-tuned reflectarray," *IEEE Transactions on Antennas and Propagation*, vol. 61, no. 2, pp. 635–645, 2013.

[7] S. Costanzo, F. Venneri, A. Raffo, G. Di Massa, and P. Corsonello, "Radial-shaped single varactor-tuned phasing line for active reflectarrays," *IEEE Transactions on Antennas and Propagation*, vol. 64, no. 7, pp. 3254–3259, 2016.

[8] N. I. Dzulkipli, M. H. Jamaluddin, R. Gillard et al., "Mutual coupling analysis using FDTD for dielectric resonator antenna reflectarray radiation prediction," *Progress In Electromagnetics Research B*, vol. 41, pp. 121–136, 2012.

[9] M. Zhou, S. B. Sørensen, E. Jørgensen, P. Meincke, O. S. Kim, and O. Breinbjerg, "Analysis of printed reflectarrays using extended local periodicity," *Proceedings of the 5th European Conference on Antennas and Propagation (EUCAP)*, 2011, pp. 1494–1498, Rome, Italy, 2011.

[10] S. Costanzo, F. Venneri, and G. Di Massa, "Bandwidth enhancement of aperture-coupled reflectarrays," *IEE Electronics Letters*, vol. 42, no. 23, pp. 1320-1321, 2006.

[11] F. Venneri, S. Costanzo, and G. Di Massa, "Bandwidth behavior of closely spaced aperture-coupled reflectarrays," *International Journal of Antennas and Propagation*, vol. 2012, Article ID 846017, 11 pages, 2012.

[12] S. Costanzo and F. Venneri, "Miniaturized fractal reflectarray element using fixed-size patch," *IEEE Antennas and Wireless Propagation Letters*, vol. 13, pp. 1437–1440, 2014.

[13] S. Costanzo, F. Venneri, G. Di Massa, A. Borgia, A. Costanzo, and A. Raffo, "Fractal reflectarray antennas: state of art and new opportunities," *International Journal of Antennas and Propagation*, vol. 2016, Article ID 7165143, 17 pages, 2016.

[14] D. Oloumi, S. Ebadi, A. Kordzadeh, A. Semnani, P. Mousavi, and X. Gong, "Miniaturized reflectarray unit cell using fractal-shaped patch-slot configuration," *IEEE Antennas and Wireless Propagation Letter*, vol. 11, pp. 10–13, 2011.

[15] R. Deng, S. Xu, F. Yang, and M. Li, "Single-layer dual-band reflectarray antennas with wide frequency ratios and high aperture efficiencies using Phoenix elements," *IEEE Transactions on Antennas and Propagation*, vol. 65, no. 2, pp. 612–622, 2017.

[16] P. Y. Qin, Y. J. Guo, and A. R. Weily, "Broadband reflectarray antenna using subwavelength elements based on double square meander-line rings," *IEEE Transactions on Antennas and Propagation*, vol. 64, no. 1, pp. 378–383, 2016.

[17] L. Guo, P. K. Tan, and T. H. Chio, "Beam-scanning improvement of reflectarrays using single-layered sub-wavelength elements," in *2015 IEEE 5th Asia-Pacific Conference on Synthetic Aperture Radar (APSAR)*, pp. 131–134, Singapore, 2015.

[18] J. L. T. Ethier, D. A. McNamara, M. R. Chaharmir, and J. Shaker, "Reflectarray design with similarity-shaped fragmented sub-wavelength elements," *IEEE Transactions on Antennas and Propagation*, vol. 62, no. 9, pp. 4498–4509, 2014.

[19] A. Edalati and K. Sarabandi, "Wideband reflectarray antenna based on miniaturized element frequency selective surfaces," *2012 6th European Conference on Antennas and Propagation (EUCAP)*, 2011, pp. 362–364, Prague, Czech Republic, 2011.

[20] F. Costa and A. Monorchio, "Closed-form analysis of reflection losses in microstrip reflectarray antennas," *IEEE Transactions on Antennas and Propagation*, vol. 60, no. 10, pp. 4650–4660, 2012.

[21] D. M. Pozar and T. A. Metzler, "Analysis of a reflectarray antenna using microstrip patches of variable size," *Electronics Letters*, vol. 29, no. 8, p. 657, 1993.

[22] J. P. Gianvittorio and Y. Rahmat-Samii, "Fractal antennas: a novel antenna miniaturization technique, and applications," *IEEE Antennas and Propagation Magazine*, vol. 44, no. 1, pp. 20–36, 2002.

[23] J. Anguera, J. P. Daniel, C. Borja et al., "Metallized foams for antenna design: application to fractal-shaped Sierpinski-carpet monopole," *Progress In Electromagnetics Research*, vol. 104, pp. 239–251, 2010.

[24] C. A. Balanis, *Antenna Theory Analysis and Design*, Wiley, New York, NY, USA, 1989.

[25] "Ansoft Designer®".

[26] S. Costanzo, F. Venneri, G. Di Massa, and G. Angiulli, "An improved synthesis algorithm for reflectarrays design," *IEEE Antennas and Wireless Propagation Letters*, vol. 4, no. 4, pp. 258–261, 2005.

[27] J. Perruisseau-Carrier, *Microwave Periodic Structures Based on Microelectromechanical Systems (mems) and Micromachining Techniques, [Ph.D. Thesis]*, EPFL Scientific Publications, 2007.

[28] C. A. Balanis, *Advanced Engineering Electromagnetics*, Wiley, New York, NY, USA, 1997.

[29] F. Venneri, S. Costanzo, and G. Di Massa, "Fractal-shaped metamaterial absorbers for multireflections mitigation in the UHF band," *IEEE Antennas and Wireless Propagation Letters*, vol. 17, no. 2, pp. 255–258, 2018.

[30] LPKF Laser & Electronics, "LPKF ProtoMat," https://www.lpkf.com/.